WHITE-LIGHT AND RADIO SOUNDING OBSERVATIONS OF CORONAL TRANSIENTS

M. K. BIRD and H. VOLLAND
Radioastronomisches Institut, Universität Bonn, 5300 Bonn, F.R.G.

R. A. HOWARD, M. J. KOOMEN, D. J. MICHELS, and N. R. SHEELEY, Jr.
Naval Research Laboratory, Washington, DC 20375, U.S.A.

J. W. AMSTRONG, B. L. SEIDEL, C. T. STELZRIED, and R. WOO
Jet Propulsion Laboratory, Pasadena, CA 91103, U.S.A.

(Received 24 October, 1984; in revised form 23 April, 1985)

Abstract. A concerted search for coronal transients was conducted with the 'Solwind' coronagraph during the solar occultations of the two Helios spacecraft in October/November 1979. The polarization angle and bandwidth of the linearly polarized S-band downlink signal were monitored at the three 64-m tracking stations of the NASA Deep Space Network to determine coronal Faraday rotation and spectral broadening. A one-to-one correspondence could be established between abrupt disturbances in the two signal parameters and the passage of a white-light transient through the signal ray path from spacecraft to Earth. The white-light morphology and the additional information provided by the radio sounding coverage are presented for each of the five distinct events recorded. Although no specific example could be observed in sufficient detail in both white light and Faraday rotation to derive the small-scale magnetic structure, some qualitative descriptions of the orientation and rough estimates of the magnitude of the transient magnetic field could be made.

1. Introduction

The coronal mass ejection event (CME), a phenomenon sometimes also referred to loosely as a 'coronal transient', has been extensively studied since the availability of white-light observations from orbiting coronagraphs. Following the earlier successes of OSO-7 and Skylab, the SMM Coronagraph/Polarimeteter (House *et al.*, 1981; Wagner *et al.*, 1981) and the 'Solwind' coronagraph (Sheeley *et al.*, 1980a, b) have greatly extended the observational data base for further study and understanding of the dynamic corona (see also the recent review by Dryer, 1982).

One of the more obvious remaining uncertainties in describing the dynamics of CMEs is the orientation and strength of the magnetic field in and around the transient material. Although only about one-third of the CMEs are generally described as 'loop-like' (MacQueen, 1980; Wagner, 1984), most theoretical efforts have been concentrated on this one particular variety of coronal transient (Mouschovias and Poland, 1978; Pneuman, 1980, 1983; Low, 1981; Anzer and Pneuman, 1982; and Yeh, 1982). Most of these treatments have assumed the magnetic field to thread the visible loop in the form of a helix either with or without a significant azimuthal component. The numerical simulations of coronal transients (e.g. Steinolfson *et al.*, 1978; Wu *et al.*, 1981) conform

Solar Physics **98** (1985) 341–368. 0038–0938/85.15.

with the hypothesis that coronal transients are basically spherical in shape and present an illusory loop appearance only due to the line-of-sight effect at the solar limb. The observation of a spherical coronal transient directed at Earth (Howard *et al.*, 1982), the association of an interplanetary magnetic cloud with a CME (Burlaga *et al.*, 1982), and the polarization analysis of Crifo *et al.* (1983) all provide evidence for the existence of 'bubble-like' CME events. The magnetic structure throughout the compression region of a spherically shaped transient would most likely not be helical as in the case of a loop.

The rather sparse empirical information on the transient magnetic field has been derived thus far from transient-associated radio burst emission. Dulk *et al.* (1976), assuming a gyrosynchrotron source, estimate a magnetic field strength (no directional information) for the compression region of the Skylab transient of 14/15 September 1973 of 0.7 G at a coronal height of 3.1 $R_{\odot}$. Radio emission from a white-light loop observed by Gergely *et al.* (1981) was similarly interpreted and found to imply a magnetic field magnitude of 2–4.5 G at a solar distance of 2.1 $R_{\odot}$. Stewart *et al.* (1982) infer a lower bound of 0.6 G for the confining field strength of a dense underlying plasmoid (not the transient's leading edge) at the coronal height $2.5_{\odot}$.

The possibility of measuring the 'magnetic profile' of a CME using the linear-polarized radio signal of a spacecraft located at solar superior conjunction was discussed by Bird *et al.* (1980). The mean transient magnetic field component along the line-of-sight between spacecraft and Earth can be obtained by simultaneously measuring the change in Faraday rotation of the radio signal and the change in electron content as derived from white-light coronagraph variations during the passage of the CME through the signal ray path. The Faraday rotation signature across the CME might be expected to display different characterizing features, for example, if the general morphology were bubble-like or loop-like. The electron content measurements are necessary for separating the magnetic field and electron density contributions to the signal Faraday rotation.

This paper describes the most extensive joint coronagraph and radio sounding observations ever conducted during the solar occultation of an interplanetary spacecraft. Faraday rotation (FR) and spectral broadening (SB) measurements were made with the two Helios spacecraft during their superior conjunctions in October (Helios 2) and November (Helios 1) of 1979. These radio sounding data were recorded at the three 64-m stations of the NASA Deep Space Network (DSN). The 'Solwind' coronagraph monitored the white-light corona, as often as possible in the maximum data rate mode, in support of the Helios radio science measurements. Helios 1 (and Helios 2 up to March 1980) has been sampling the interplanetary medium over the past few years, primarily at positions off the east or west solar limbs. This is the optimum location for the detection of the interplanetary signatures of the white-light CMEs observed by 'Solwind'. Almost all suitably directed mass ejections were found to be associated with shocks at Helios (Schwenn, 1983; Sheeley *et al.*, 1983). This study uses Helios as a radio probe during the brief periods when the spacecraft moves behind the Sun from west limb to east limb. Five well-defined coronal transients were detected both in white light and the radio sounding data during approximately 12 days of observations during these periods.

Two previous papers have addressed specific aspects of these joint observations. Woo *et al.* (1982) pointed out that the bandwidth of the Helios signal was broadened prior to passage of the leading edge of the white-light event through the signal ray path on 24 October, 1979. Bird *et al.* (1984) concluded that the five favorably directed white-light CMEs were correlated one-to-one with abrupt disturbances in Faraday rotation, and are thus very likely different manifestations of the same phenomenon. The main purpose of this present work is to derive estimates of the magnetic field in those coronal transients sounded with the Helios radio signal during the solar occultations of 1979. Although ubiquitous data gaps both in the Faraday rotation and the coronagraph data have limited the extent of the analysis, credible values for the *mean longitudinal component* of the transient magnetic field of the order of 10–100 mG at $R = 2.5\ R_\odot$ are obtained. These values were found to exceed the inferred (radial) magnetic field *magnitude* in the pre-transient ambient corona.

2. White-Light and Radio Sounding Data for each Event

The coronograph images and, where appropriate, the corresponding height-time diagram and radio sounding data are presented below for each of the five documented transient events during the Helios solar occultations in 1979. The measurement error for the (projected) radial position of the CMEs from the 'Solwind' images ranges from $\pm 0.3\ R_\odot$ to $\pm 1.0\ R_\odot$, resulting in relatively large uncertainties in the derived transient speeds. Although modest accelerations or decelerations cannot be excluded, the motion of all CMEs observed here was found to be consistent with a constant outward expansion as indicated by the linear fit in each height-time diagram. Figures showing the solar elongation angle (solar offset) of the Helios probes and an overview of the observed Faraday rotation during the two occultations have been presented in Bird *et al.* (1984).

Helios 2: 23 October, 1979

Figure 1 shows a series of 'Solwind' difference images, constructed by subtracting an earlier pre-transient coronagraph image ('base' image) from the image taken at the indicated UT times. The base images in this case were taken from a series beginning at 03 : 07 UT, i.e. during a quiet interval well before the appearance of a white-light transient. The field of view of the images extends from the outer edge of the external occulting disk at about $2.6\ R_\odot$ out to $8\ R_\odot$. The actual size of the photosphere is indicated in the first image of the sequence at upper left. The apparent position of Helios 2, indicated by the dot in the small white circle, moves from $8.1\ R_\odot$ at 06 : 20 UT to $7.1\ R_\odot$ in the last image at 14 : 55 UT. This corresponds to an apparent velocity of 22 km s^{-1} or $2.7\ R_\odot$ per day.

The west-limb brightening in Figure 1 between $\pm 20°$ solar latitude is an outwardly propagating coronal transient that displays a brighter core underneath its leading edge. The coronal heights of these two positions of relatively high contrast were determined from the first five images in Figure 1 plus three additional images not shown and are

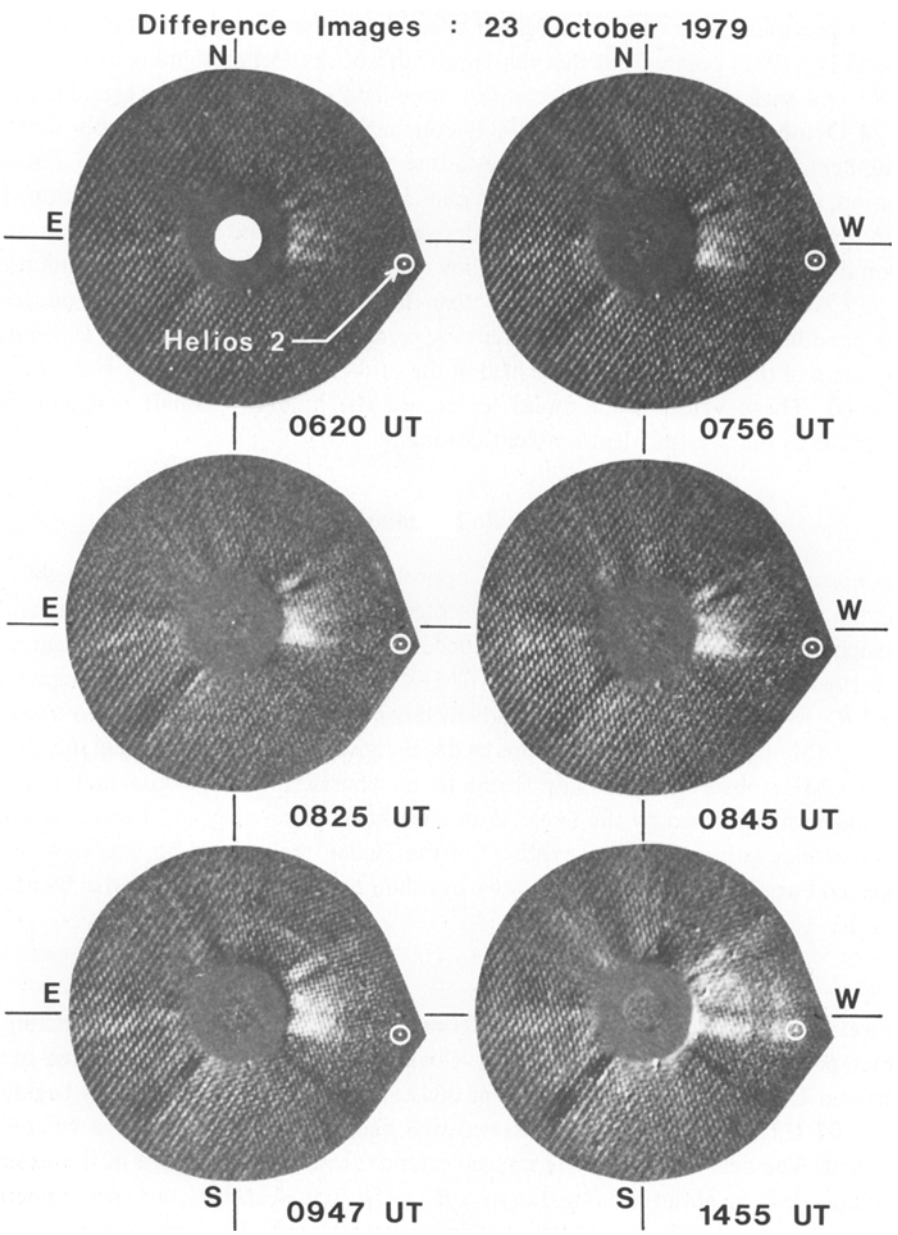

Fig. 1. Difference images of the corona during the transient of 23 October, 1979. The base images were taken from the pre-transient orbit that began at 03 : 07 UT. The position of Helios 2 is indicated by the dot in the white circle. The field of view extends from the edge of the occulting disk at about 2.6 $R_\odot$ to about 8 $R_\odot$. The actual size of the Sun is shown in the first image at upper left.

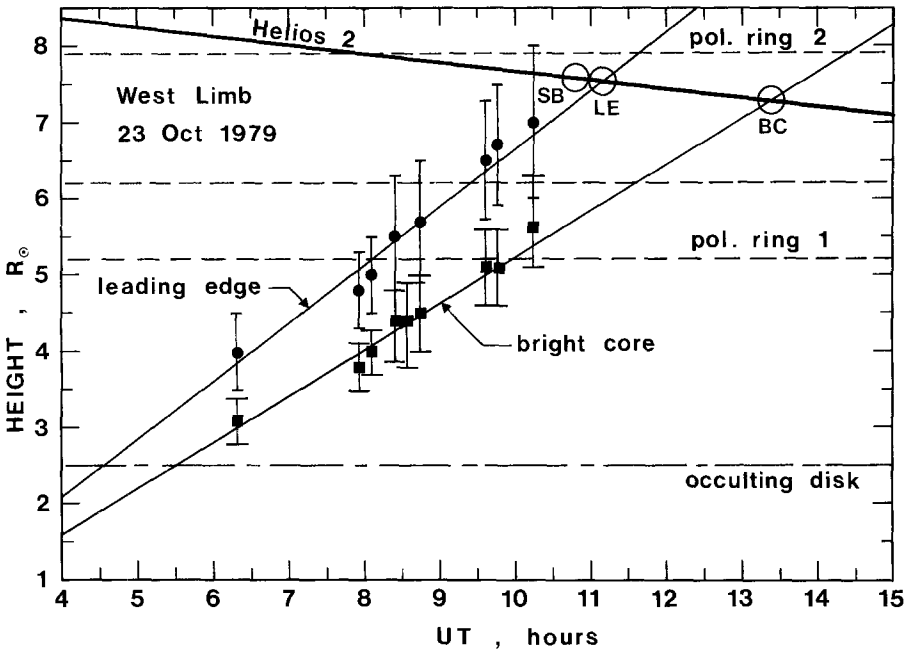

Fig. 2. Height-time diagram of the coronal transient of 23 October, 1979. The velocity of the leading edge of the event is ca. 145 km s^{-1}. The first increase in spectral broadening at time t = SB (10 : 50 UT) occurred just prior to the most probable time of arrival of the leading edge (t = LE) at the Helios ray path. This event was found to have a bright core that moved outward at a slightly lower velocity (115 km s^{-1}) than the leading edge.

displayed in the height-time diagram of Figure 2. The radial position and width of the polarizer rings, which diminish the brightness of the transient, are also indicated in Figure 2. Determinations of the radial positions of the CME are less precise when it is behind one of these rings. Although the error estimates are rather large, a linear fit of these radial positions yields a constant expansion velocity of 145 $\pm$ 70 km s^{-1} for the transient's leading edge. This results in a projected time of arrival at the Helios ray path, located at solar latitude S4.6 and solar distance 7.5 $R_\odot$, of 11 : 15 UT. This arrival time is denoted by the code 'LE'. The outer edge of the bright core moves more slowly at a velocity of 115 $\pm$ 50 km s^{-1}. The code letters 'BC' (at 13 : 30 UT) denote the most probable arrival time of this feature at the Helios ray path. Finally, the instant of the initial increase in the signal bandwith at 10 : 50 UT is marked in Figure 2 with the code 'SB'.

Figure 3 shows the radio sounding date from Helios 2 during the coronal transient of 23 October, 1979. Faraday rotation (FR) in degrees at S-band is plotted in the lower panel and spectral broadening (SB) in Hz is shown in the upper panel. The radial offset of the Helios ray path is given along the upper abscissa. The initial increase in SB is detected about 25 min prior to the most probable arrival time of the transient's leading edge at the Helios ray path (indicated by the vertical dashed line). The error box on the

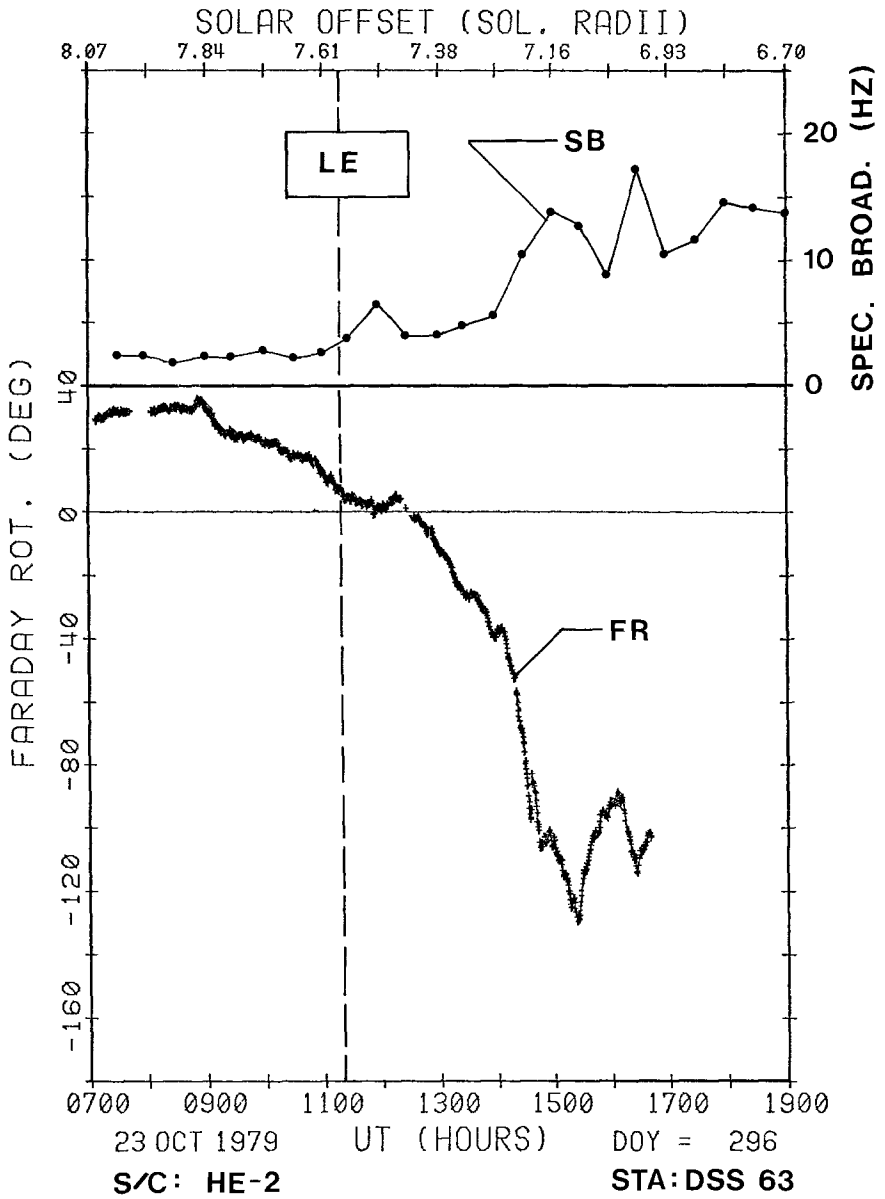

Fig. 3. Faraday rotation FR (lower panel) and spectral broadening SB (upper panel) of the Helios 2 carrier signal recorded at the DSN Madrid station DSS 63 on 23 October 1979. The apparent solar offset of Helios 2 is given at the top. A slight increase in SB occurs just prior to the most probable arrival time of the transient's leading edge at 11 : 15 UT, given by the dashed vertical line. The uncertainty in this time is indicated by the width of the box 'LE'. Larger deviations in FR and SB occurred starting at 14 : 00 UT, possibly in association with the arrival of the transient's bright core.

time 'LE', however, extends from 10 : 15 to 12 : 30 UT due to the large uncertainty in the velocity, so the exact timing of these events cannot be positively determined. The FR profile shows surprisingly little reaction to the arrival of 'LE' (ΔFR $\simeq 5°$), but both FR and SB display abrupt deviations starting at about 14 : 00 UT, which may be associated with the arrival of the denser core of the transient.

Helios 2: 24 October, 1979

A series of six 'Solwind' difference images taken during the CME of 24 October, 1979 is shown in Figure 4. The base images for this series were taken just prior to the first sighting of the transient, which emerged from behind the occulting disk at 04 : 00 UT (upper left). The apparent position of Helios 2 in the ecliptic plane moved in from the previous day to smaller solar distances (white dot in circle) at solar latitude S4.5. The west-limb CME in Figure 4 extends in latitude from N15 to S10 and is again composed of a bright core imbedded within a more diffuse white-light front. A coronal streamer at the southern edge of the CME has been displaced to the south, leaving a void along the west-limb radial at S10.

The height-time diagram of this event derived from the first five images of Figure 4 plus two other undisplayed difference images is presented in Figure 5. The letter codes 'LE' and 'BC' again denote the most probable arrival times of the leading edge and bright core of the transient at the Helios ray path. The projected velocity of the leading edge is 160 $\pm$ 50 km s^{-1} and that of the bright core is 120 $\pm$ 40 km s^{-1}. The code letters 'SB' at 05 : 00 UT mark the initial broadening of the Helios signal bandwidth in response to the CME. The most probable time of the arrival of 'LE' at the Helios ray path, located at 5.3 $R_\odot$, is 06 : 40 UT. The smaller position errors from the coronagraph images and the smaller solar distance of the Helios ray path result in a much smaller range of possible arrival times of 'LE' than for the CME of the previous day. The error box on 'LE' in this case extends from 06 : 10 to 07 : 00 UT. In contrast to the event of the previous day, therefore, the initial broadening of the Helios signal definitely occurred before the arrival of the white-light front at the signal ray path. Woo *et al.* (1982) interpret this premature broadening of the signal as due to the passage of a (weak) shock front. The transit speed ot the shock can be determined by comparing the time of 'SB' with the extrapolated 'surface event time', derived from the height-time diagram of Figure 5. Within the limits defined by the measurement errors, both the leading edge and the bright core of the white-light CME could have originated from a point at one solar radius sometine in the interval from 00 : 00–02 : 30 UT (most probable surface time: 01 : 30 UT). The slope of the indicated dashed line in Figure 5 yields a most probable projected shock velocity of about 250 km s^{-1}. Considering the uncertainty in the surface event time, shock speeds ranging from 175 km s^{-1} to 350 km s^{-1} would also be consistent with these data.

The Helios radio sounding data during this event are displayed in Figure 6. Whereas the SB trace is continuous over this interval, a system malfunction at the Canberra DSN station prevented the recording of FR data until the Madrid DSN station began its track at 07 : 00 UT. FR data are therefore unavailable during the passage of 'LE' through the

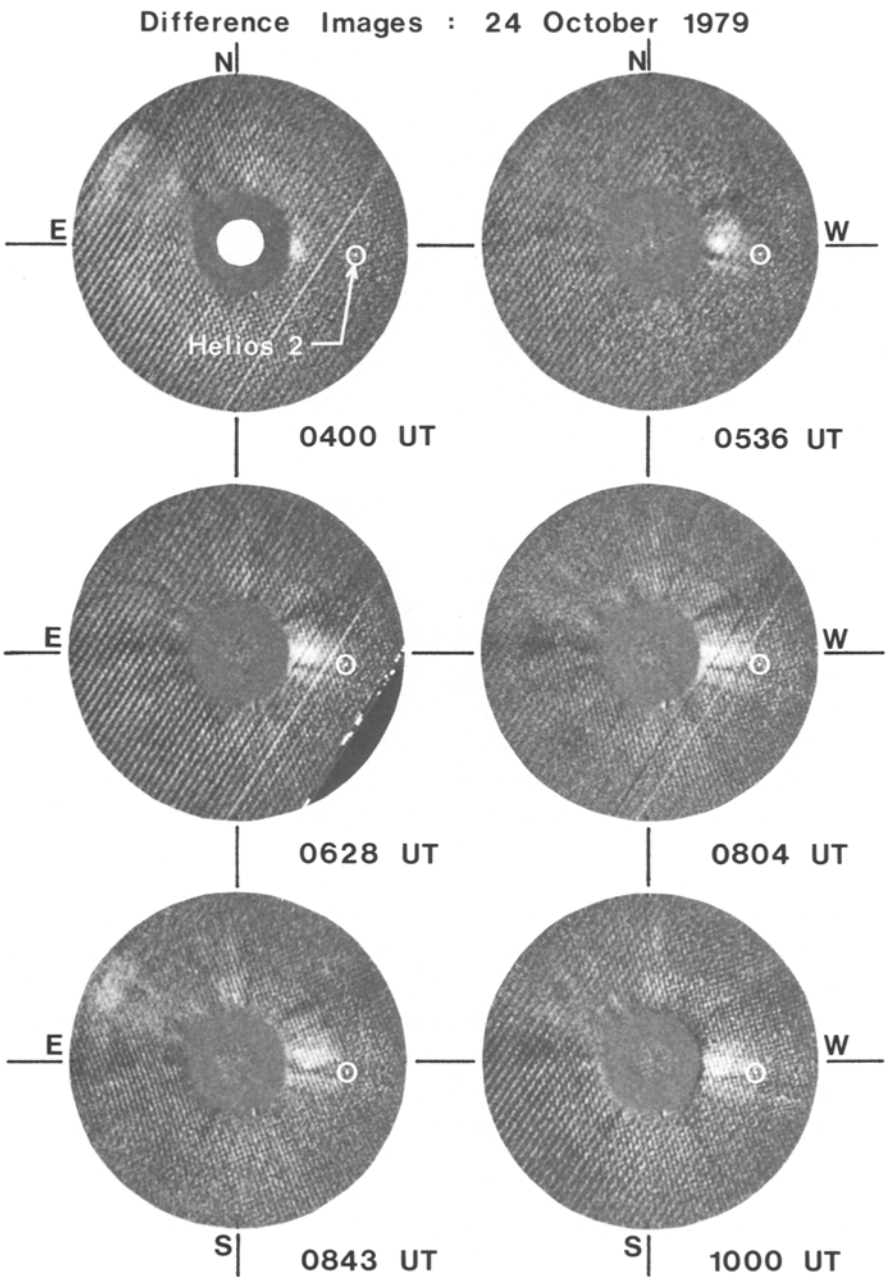

Fig. 4. Difference images of the corona during the transient of 24 October, 1979. The base image was taken from the series beginning at 03 : 16 UT, well before the onset of the transient. The apparent position of Helios 2 is again indicated by the dot in the white circle.

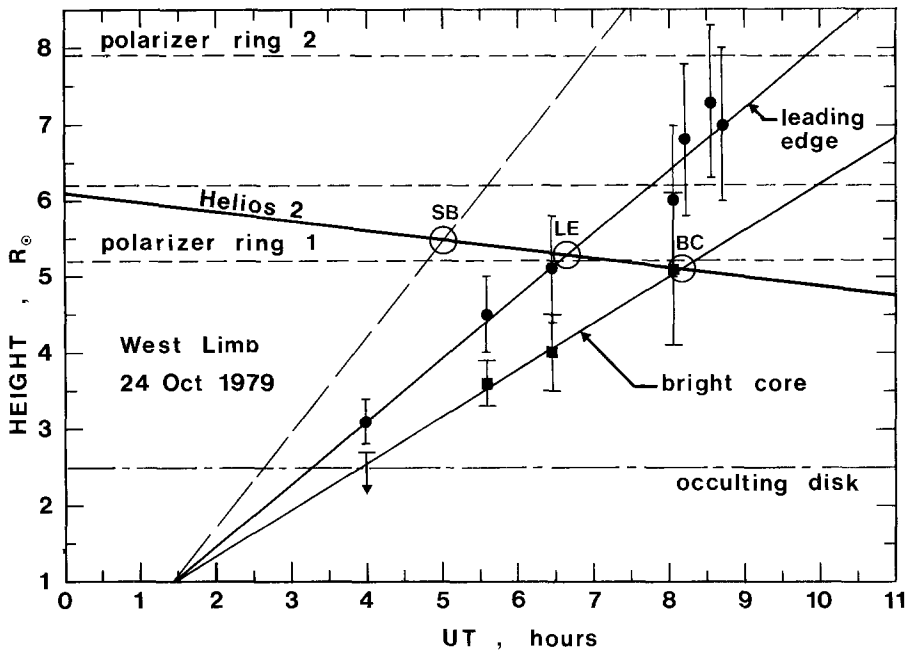

Fig. 5. Height-time diagram of the coronal transient of 24 October, 1979. The leading edge of the white-light event has a projected radial speed of 160 km s^{-1}. The bright core within the transient moves outward more slowly (ca. 120 km s^{-1}). The time t = SB at 05 : 00 UT marks the start of the disturbance in the spectral broadening data, which occurred well ahead of the projected crossing of the Helios ray path by the transient's leading edge at time t = LE (06 : 40 UT). The bright core reached the Helios ray path at t = BC (08 : 15 UT).

line-of-sight. The increase in SB, however, is plainly seen to occur well in advance of the possible range of 'LE'. When the bright core arrives at the Helios ray path at approximately 08 : 15 UT, the FR profile begins to display wild deviations of $\Delta FR \simeq \pm 50°$ with a quasi-periodic behavior about its mean background value (see also Bird *et al.*, 1984). The SB data at this time, although less obvious than during the event of the previous day (Figure 3), were definitely enhanced with respect to typical quiet corona values (see also Woo *et al.*, 1982).

Helios 2: 27 October, 1979

Tracking of Helios 2 resumed on 27 October on the east solar limb after a two-day blackout interval. Abnormal jumps in FR and SB were first recorded between 07 : 00 and 12 : 00 UT on this day and indications of transient coronal activity just south of the solar equator could be inferred from the few available coronagraph images. The 'Solwind' coverage was considerably better, however, during a distinct CME occurring about seven hours later at the same solar position angle. Figure 7 shows the relationship of this white-light transient to Helios 2 at four different times. The latitudinal extent of the brightening runs from S25 to N10. It is not certain whether the northern edge of the

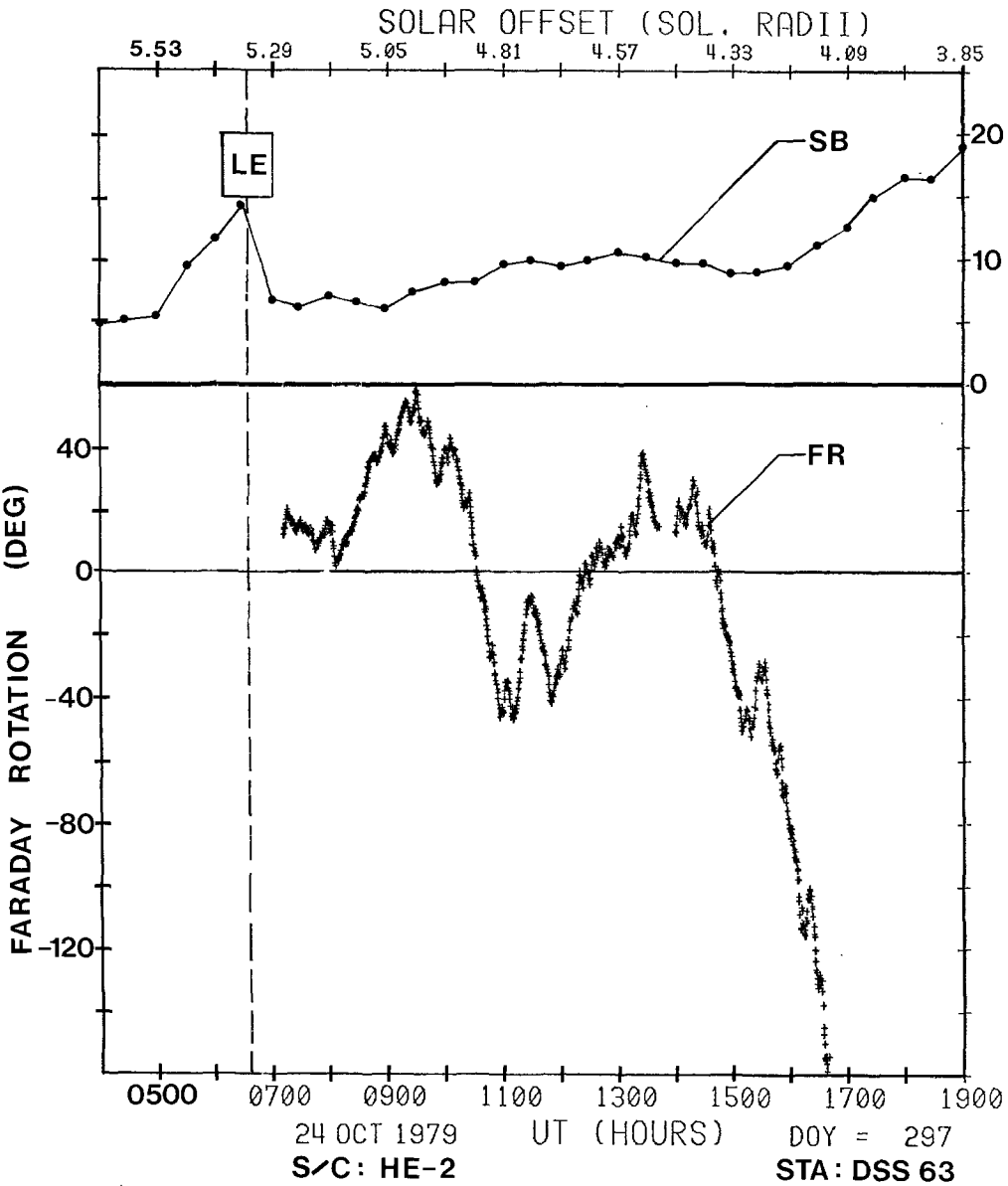

Fig. 6. Faraday rotation and spectral broadening of the Helios 2 signal during the coronal transient of 24 October, 1979. Data taken ater 07 : 00 UT were recorded at the DSN Madrid station DSS 63. The SB data prior to 07 : 00 UT were recorded at the Canberra station DSS 43. A system malfunction prevented the recording of FR data in this interval, during which the leading edge of the transient passed through the Helios/Earth line-of-sight (vertical dashed line). In this case, the increase in SB definitely occurred before the arrival of the transient's leading edge at the Helios ray path.

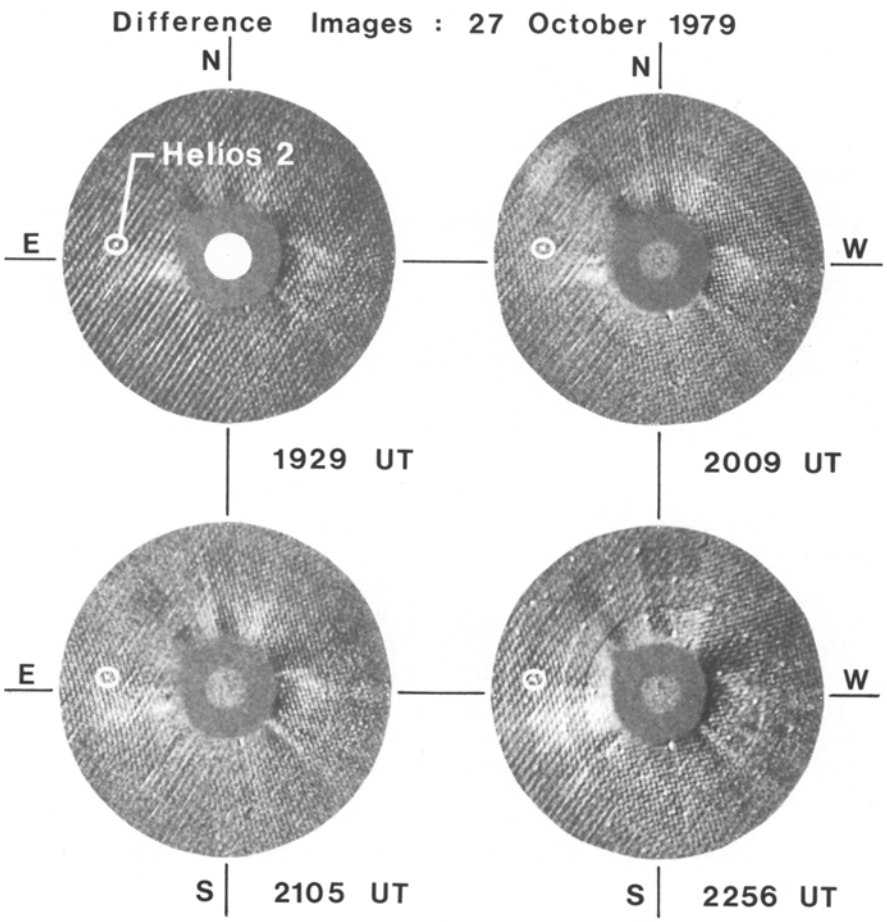

Fig. 7. Difference images of the corona during a faint east limb transient on 27 October, 1979. The base images were taken from a series starting at 14 : 40 UT. Either the extreme northern edge of the white-light transient, or perhaps a transient-induced rearrangement of the ambient corona, were responsible for the disturbances recorded with the Helios 2 signal.

CME actually eclipsed Helios 2, or if the disturbance in the signal parameters were merely caused by a rearrangement of the ambient corona. No bright core could be discerned in this case and the brightness level was also lower than the west-limb events of 23/24 October.

The height-time diagram for this event is shown in Figure 8. The expansion velocity of the leading edge was determined to be 255 km s^{-1}, but the relatively large error bars allow values between 60 and 370 km s^{-1}. The CME overtakes Helios 2, moving outward at about 26 km s^{-1}, at 20 : 50 UT ($R = 5.7\ R_{\odot}$).

The Helios radio sounding data during this event are plotted in Figure 9. The large uncertainty in the position and velocity of the transient yields a correspondingly wide error box on 'LE'. Consistent with the two west-limb events, an increase in SB appears

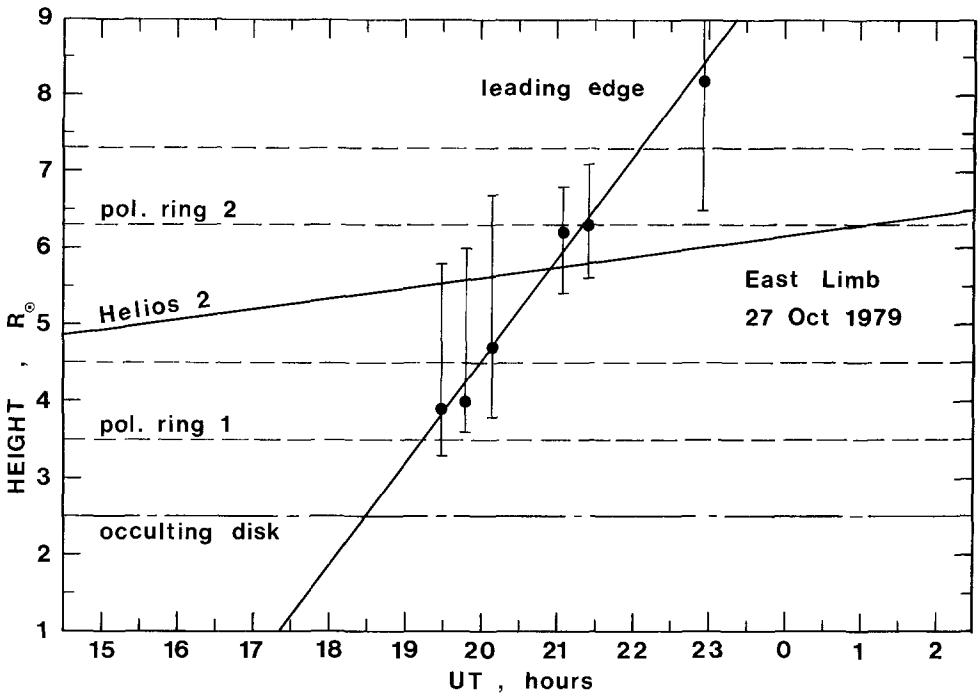

Fig. 8. Height-time diagram of the coronal transient of 27 October 1979. The velocity of the leading edge is ca. 255 km s^{-1}. It passes the Helios 2 ray path, which also moves outward at a velocity of 26 km s^{-1}, at about 20 : 50 UT.

to have occurred at ca. 20 : 00 UT, prior to the most probable arrival time of the white-light front at the Helios ray path. The exact sequencing of these events, however, is not nearly as well defined as in the case of 24 October. The FR profile shows an increase from $-40°$ to the zero level over a 90 min interval. This monotonic behavior contrasts with the events seen on the west limb, where ΔFR displayed definite reversals in sign.

Helios 1: 15/16 November, 1979

The largest dynamic coronal event during the two occultations began late on 15 November, when the proximate point on the Helios-1 ray path was located at $R = 7.1\ R_\odot$, solar latitude S6.4. As seen in the series of 12 'Solwind' images in Figure 10, the optical event actually consisted of two rapidly-moving CMEs, one north and one south of the solar equator. Height-time curves for both CMEs are shown together with the Helios-1 SB data in Figure 11. It should be noted that the projected center latitudes of these two mass ejections at N50 and S45, respectively, are well removed from the equatorial location of the Helios ray path. Unfortunately, there exist no FR data for this event due to a failure of the data recording system at the DSN Canberra station.

Other solar activity during this interval (*Solar-Geophysical Data*, November 1979), the times of which are indicated in Figure 11, includes the following: The northern CME,

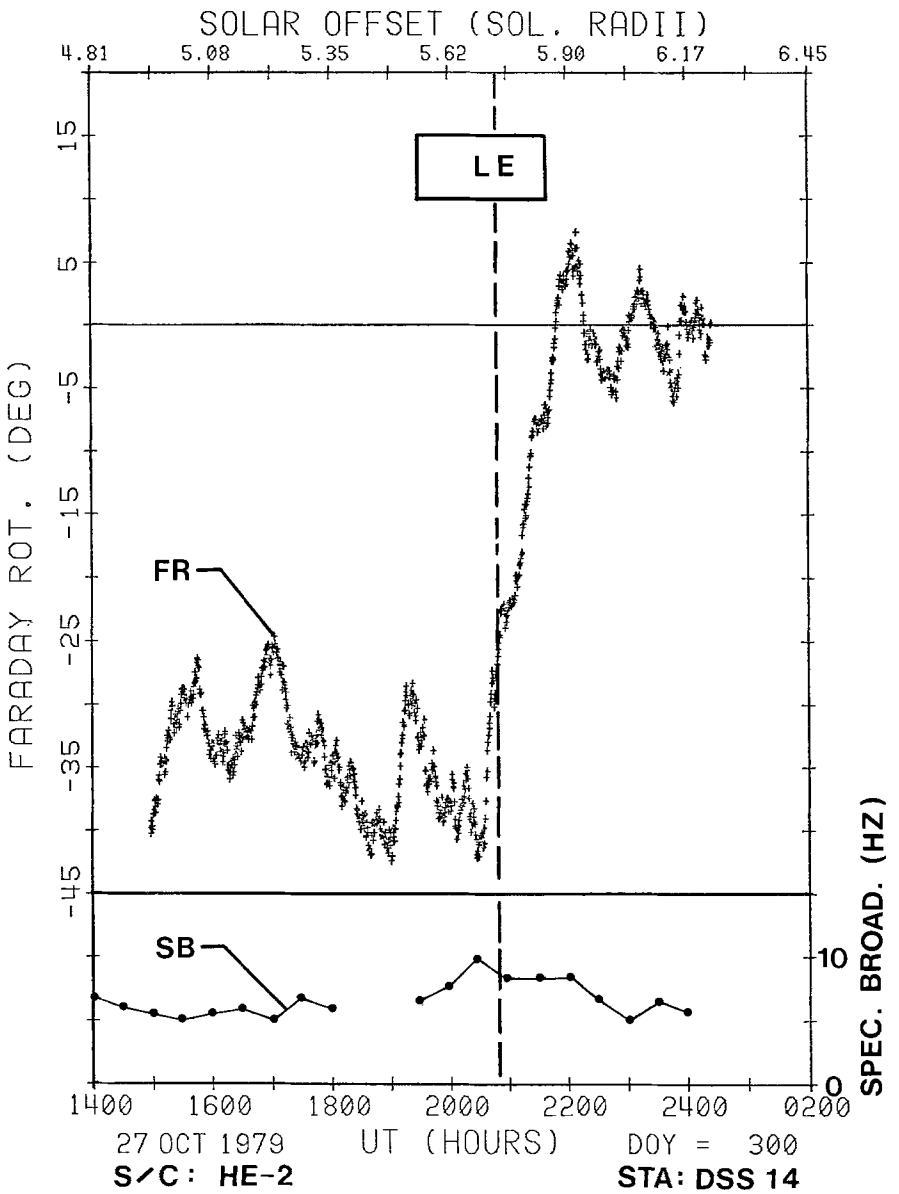

Fig. 9. Faraday rotation and spectral broadening of the Helios 2 signal during the coronal transient on 27 October, 1979. Data taken after 15 : 00 UT were recorded at the DSN Goldstone station DSS 14. The SB data again tend to show a reaction to the transient prior to the most probable arrival time at the Helios 2 ray path (vertical dashed line). The FR trace moves through 40° in about 90 min.

which occurred about one hour earlier than the southern CME, was associated with a 2B Hα-flare at (N29, W38) starting at 21 : 22 UT. A 'Great Burst' of solar 10.7 cm radiation (peak flux: 920 sfu) was recorded from 21 : 39 to 22 : 05 UT. Metric type II

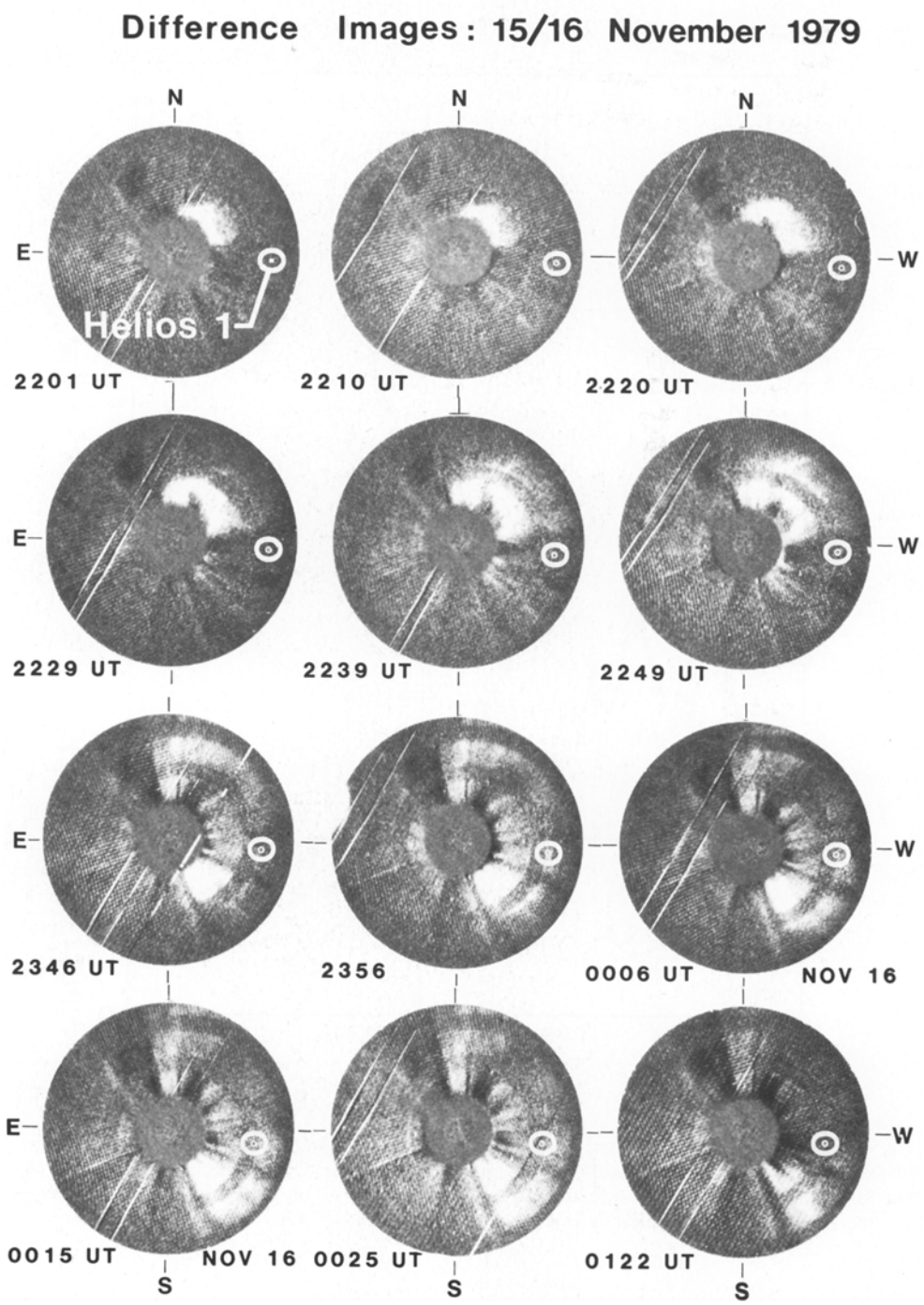

Fig. 10. Difference images during the large CME events of 15/16 November 1979. The first CME was first sighted at 22 : 01 UT at a projected west-limb latitude of N50. It was followed by a second CME on the west limb centered at S45. Helios 1 (dot in white circle), with its ray path to Earth essentially in the solar equatorial plane, still recorded large SB transients.

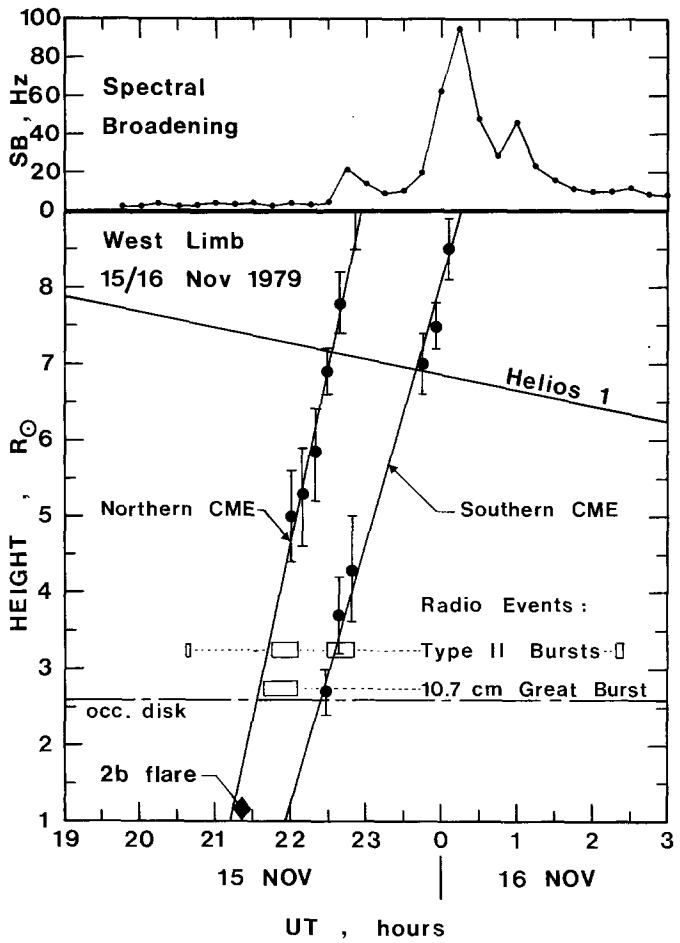

Fig. 11. Time-height diagrams of the two CMEs of 15/16 November, 1979 (lower panel) and Helios 1 spectral broadening data during the events (upper panel). Times of metric and decimetric radio bursts are shown by horizontal bars. A large Hα-flare (2B) occurred at 21 : 22 UT. Projected speeds of the CMEs: ca. 900 km s^{-1} (north); ca. 660 km s^{-1} (south). Note that the positions of the two CMEs and Helios 1 are well separated in latitude.

bursts observed at Culgoora were also undoubtedly associated with this CME 'double' (see also Sheeley *et al.*, 1984).

The projected speed of the northern CME was determined to be 900^{+250}_{-150} km s^{-1}. The maximum latitudinal extent of the white-light event (at ca. 22 : 49 UT) was from N05 to N100 (i.e. 10° over onto the east limb). This range does *not* include the Helios-1 ray path, which moved in slowly along the radial at ca. 40 km s^{-1}. The CME reaches the coronal height of Helios 1 (7.1 $R_\odot$) in the interval 22 : 29 to 22 : 35 UT, but no transient material can be seen at the Helios 1 latitude at this time (Figure 10: images at 22 : 29 and 22 : 39 UT). Nevertheless, a significant increase in the signal bandwidth began at about 22 : 30 UT, reaching a relative maximum of 20 Hz at 22 : 45 UT. This

spectral broadening enhancement could thus be attributed to the passage of a shock wave, albeit much faster and stronger than the event seen earlier on Helios 2 (Woo *et al.*, 1982).

The southern CME was evidently not flare-related. Its projected velocity was estimated to be 660 $\pm$ 100 km s^{-1}, and its latitudinal range extended from S20 to S60. The Helios-1 bandwidth reached a peak of almost 100 Hz at 00 : 15 UT (16 November), at which time excess coronal material can definitely be observed at the position of Helios 1 (lower left image, Figure 10). Since the northern boundary of this CME seems to be located at S20, this excess material may be a quasi-stationary compression of the ambient corona, displaced northward by the emergence of the southern CME.

Helios 1: 16 November, 1979

Figure 12 summarizes the available coronagraph data for this last coronal transient seen in the Helios radio sounding data in 1979. In spite of the generally increased white-light coverage in support of the Helios occultations, this event did manage to escape direct detection due to an image gap from 09 : 23 to 14 : 12 UT. The two images taken at these times are shown in the upper row of Figure 12. The difference image formed from this pair is shown in the center. The remnants of what may be the base and legs of a white-light CME between latitudes N5 and S25 are the most prominent features of this and the subsequent difference images in the lower row of Figure 12. Another possibility is that the Helios ray path was eclipsed by a dynamic streamer, shoved back and forth by an actively evolving corona. The emission features in the 'Solwind' difference images of Figure 12 would also be consistent with this interpretation. After Helios tracking was terminated at about 16 : 30 UT, a large loop transient was detected by 'Solwind' over the solar north pole (last image in Figure 12).

No height-time diagram can be plotted for this case, but the instant of arrival of the disturbance at the Helios ray path can be pinpointed from the radio sounding data in Figure 13. The discontinuities in the FR and SB profiles occur almost simultaneously. The transient first produced a negative FR starting at about 12 : 05 UT, indicating a mean magnetic field within the transient oriented away from the observer. After about 10 min, the ΔFR changed sign, indicating a mean field pointing toward the observer. The bandwidth reached a relatively high value of about 40 Hz, later increasing to a second maximum of about 35 Hz. This double-peak structure in the SB data is reminiscent of the event reported by Woo and Armstrong (1981) with Voyager 1.

3. Observational Overview

With only five empirical cases available for analysis, each one under different geometrical occultation conditions, it is not possible to construct a generalized model of the 'typical' Faraday rotation (or 'typical' magnetic structure) of a coronal transient. Since none of the events could be observed in its entirety with both white-light and Faraday rotation data, a high-resolution magnetic field profile through a CME could not be derived. It should also be recognized that the three CMEs observed by 'Solwind' in October

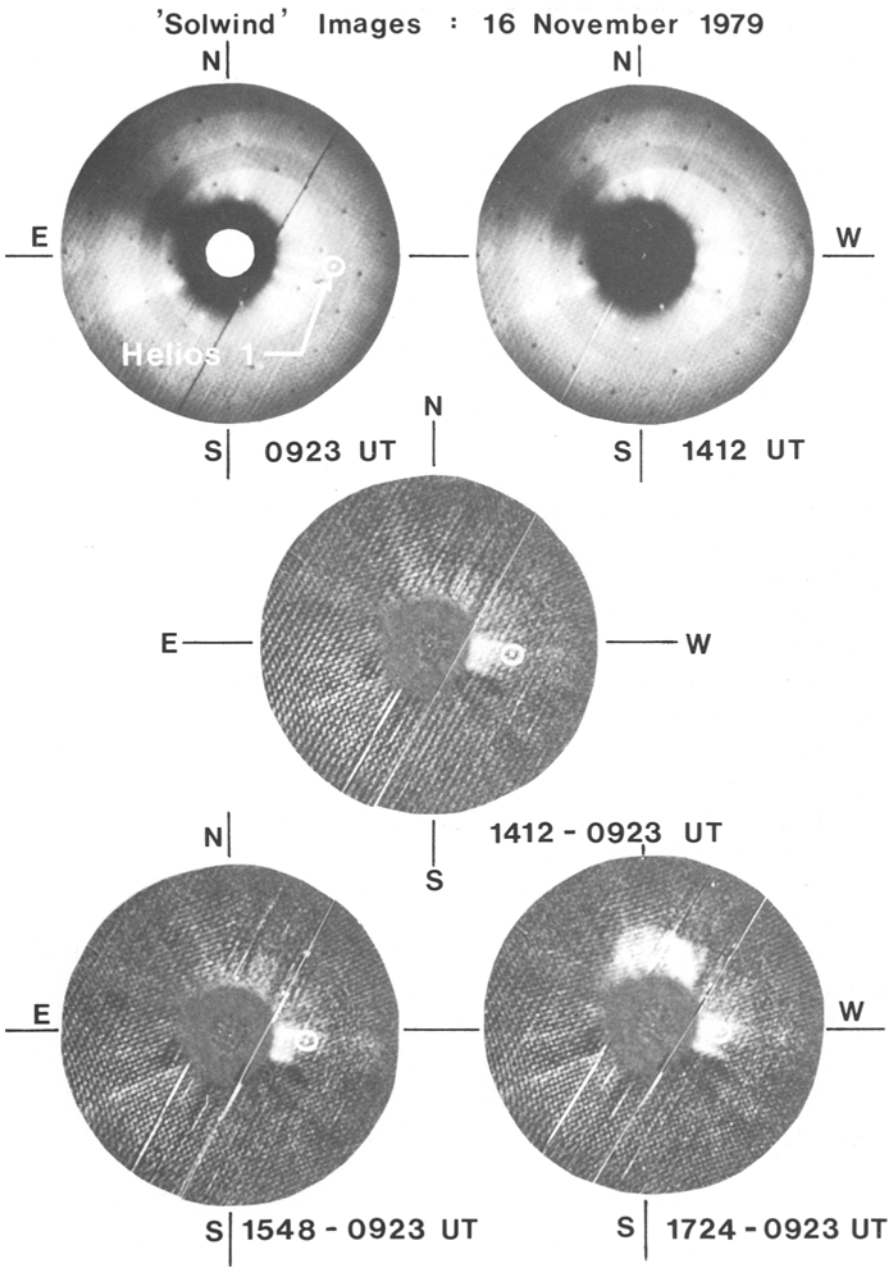

Fig. 12. 'Solwind' coronagraph images taken on 16 November, 1979. *Upper row*: direct coronal images taken before and after passage of the transient through the Helios 1 ray path: *Middle* and *lower rows*: difference images that use the base image at 09:23 UT (upper left). The position of Helios 1 is given by the dot in the white circle. Only the base and legs of a west limb transient can be seen starting with the image at 14:12 UT. A well-developed loop transient appears over the solar north pole in the last image at 17:24 UT.

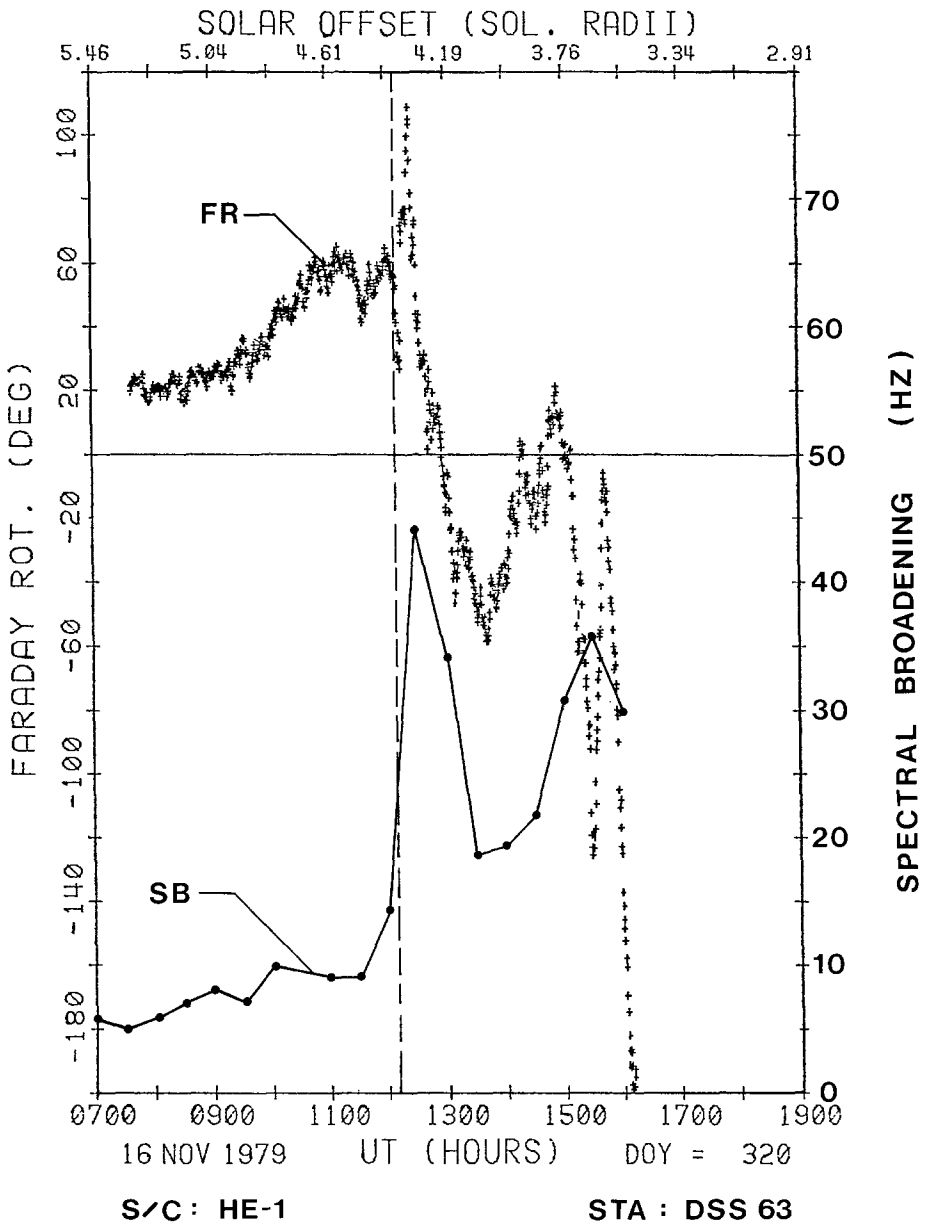

Fig. 13. Faraday rotation and spectral broadening of the Helios 1 signal during the tracking pass at DSS 63 (Madrid) on 16 November, 1979. Both signal parameters are disturbed here almost simultaneously, in contrast to the events observed with Helios 2 in October 1979.

(Helios 2 occultation) could all be classified as rather minor events according to the rating scheme of Howard *et al.* (1984). Unfortunately, no direct determinations of the transient magnetic field could be made for the more energetic events seen during the occultation of Helios 1.

In spite of these limitations, the line-of-sight component of the magnetic field in the transient could be computed for various specific times using the Helios-2 FR data and a 'Solwind' estimate of the surplus electron content extrapolated in time and space to the known location of the Helios ray path. In addition to this analysis, the description and results of which are presented in the next section, four significant aspects of these observations should be pointed out here and discussed in more detail:

(1) All white-light CMEs, at some time during their passage through or near the Helios ray path, produced abrupt, large-amplitude disturbances in the recorded signal parameters SB and FR. In fact, the only obvious commonality among the events observed here was the time scale and magnitude of variations in the Helios radio sounding data. The quiescent corona, particularly at small solar elongations, is capable of producing large variations in FR or SB, but only on time scales of hours to days. Superimposed on this slow variation are omnipresent FR and SB fluctuations with characteristic periods of minutes to hours, but with only moderate amplitudes (ΔFR $\simeq 2°$; ΔSB $\simeq 0.5$ Hz at R = 5 $R_\odot$). The variations in FR and SB associated with the CMEs observed here, however, occurred over time scales of seconds to minutes and greatly exceeded the background fluctuations im amplitude (ΔFR $\simeq 50°$; ΔSB $\simeq 10$ Hz at $R = 5\ R_\odot$).

(2) For those intervals of simultaneous FR and SB data, the degree of disturbance was not always the same for the two signal parameters. The passage of the transient's leading edge through the Helios line-of-sight on 23 October, for example, increased the SB by a factor of two, but caused only a small change in the signal's FR. The large variations in FR recorded when the bright core of the 24 October transient eclipsed the Helios ray path, on the other hand, were accompanied by only a slight enhancement in SB. This behavior can be attributed to the different physical quantities in the CME that affect these two signal parameters. The Faraday rotation, for example, fulfills the proportionality

$$\mathrm{FR} \sim \overline{B}_L N_T, \tag{1}$$

where $\overline{B}_L$ is the weighted mean magnetic field component along the signal ray path, and N_T is the total electron content along that same ray path. The spectral broadening of the Helios signal in an isotropic, turbulent corona with a Kolmogorov density fluctuation spectrum has been shown by Woo (1977) to vary as

$$\mathrm{SB} \sim \sigma_N V_P, \tag{2}$$

where σ_N is the rms electron density fluctuation and V_P is the plasma velocity perpendicular to the ray path, both evaluated at the position along the ray path of greatest electron density (usually the solar proximate point). Transient disturbances in SB without a similar reaction in FR would thus be most easily interpreted as being caused by fast-moving CMEs (high V_P) and/or CMEs with small B_L. The alternative explanation, large σ_N and small N_T, would be difficult to attain since both σ_N and N_T are generally proportional to the electron density level. Conversely, a slow CME of relatively uniform density could produce a large ΔFR with only moderate ΔSB if the

transient's magnetic field were (a) strong enough, and (b) directed along the signal ray path.

(3) Additional evidence was found for premature response of the SB to white-light CMEs observed to pass through or near the Helios ray path. Woo *et al.* (1982) first called attention to this effect for the Helios-2 event of 24 October. Although the positional measurement errors of the white-light front for the Helios-2 events of 23 and 27 October are too large for an unambiguous determination of the timing sequence, transient increases in SB did tend to occur prior to the most probable arrival time at the Helios ray path. A more convincing example could be found in the northern white-light CME of 15/16 November, which produced an abrupt increase in SB at a time when no transient material could be observed along the Helios ray path.

(4) FR time profiles were observed which indicate polarity reversals of the transient magnetic field. Previously recorded Faraday rotation transients on Pioneer 6 (Levy *et al.*, 1969) and Helios (Bird *et al.*, 1977) were found to be generally monopolar, i.e. the sign of the disturbed FR remained more or less unchanged over the duration of the transient. Indications of both positive and negative deviations were seen in the Helios 2 events of 23 October and (especially) 24 October. Considering the time scales of the quasi-periodic variations in FR (2–3 hr) and the known projected velocities of the white-light CMEs (ca. 150 km s^{-1}), the radial extent of the coronal magnetic structures associated with these events can be estimated to be $2\,R_\odot$ or even larger. In contrast, the unusual FR profile observed just after 12 : 00 UT on 16 November (Helios 1) displays polarity reversals over much smaller time scales, a behavior which might be explained by the outward propagation of a slender magnetic flux tube (thickness $\simeq 0.7\,R_\odot$) with an azimuthal (i.e. maximum longitudinal) magnetic field of ca. 1 mG (Bird *et al.*, 1980).

4. Estimates of the Transient Magnetic Field

As mentioned in the previous section, a highly-resolved determination of the magnetic structure in the CME was not possible. Only for the two transient events of 23 and 24 October (Helios 2) was the radio sounding and white-light coverage sufficient for a more detailed analysis. The line-of-sight component of the transient magnetic field is determined here during a three-hour interval for each event.

The change in Faraday rotation of the spacecraft signal due to the additional transient material in the line-of-sight is given by (see also Bird *et al.*, 1980)

$$\Delta\mathrm{FR} = K \int_t (n_t \mathbf{B}_t - n_0 \mathbf{B}_0)\,\mathrm{ds} \quad \mathrm{deg}\,, \tag{3}$$

where

$$K = 2.58 \times 10^{-13} \qquad \text{(cgs units)},$$

$$n = \text{electron density} \quad (\mathrm{cm}^{-3}),$$

$\mathbf{B}$ = magnetic field (gauss),

ds = path element (cm).

The constant K in (3) is the same in either cgs or SI units. The integral in (3) is taken along the signal ray path over the thickness of the transient. It is assumed that the values of n and $\mathbf{B}$ outside the transient are quasi-static. The transient Faraday rotation ΔFR is thus the difference between the actually measured Faraday rotation (due to contributions along the entire line-of-sight) and a 'background Faraday rotation' extrapolated from the pre-transient time profile. Transient values of n and $\mathbf{B}$ are denoted by the index 't'; pre-transient (ambient) values by the index '0'.

In order to effectively utilize the coronagraph data in evaluating (3), it is necessary to introduce the *excess* electron density given by

$$\Delta n = n_t - n_0 \,. \tag{4}$$

This is appropriate, because it is the *excess* electron content in the transient that is derived from the difference images. The unsubtracted images cannot be directly applied in this analysis, since they yield the electron content along the entire line-of-sight. Substituting (4) into (3) results in a sum of three integrals:

$$\Delta\mathrm{FR} = K \int_t (\Delta n \mathbf{B}_t + n_0 \mathbf{B}_t - n_0 \mathbf{B}_0)\,\mathrm{ds} \quad \mathrm{deg}\,. \tag{5}$$

The first term in (5) is intuitively dominant if density and magnetic field enhancements of the order of ten are typical for CMEs. Increases of this magnitude were inferred for the events discussed by Dulk *et al.* (1976) and Gergely *et al.* (1981). It is shown in the appendix that the second term of (5) is indeed smaller than the first term for the two transient events studied here. Including this term was found to decrease the magnitude of the magnetic field estimates by ca. 40%. The third term of (5) was found to be negligible. Retaining only the first term of (5), the transient Faraday rotation can be approximated by

$$\Delta\mathrm{FR} = K\overline{B}_L \Delta N_t \,, \tag{6}$$

where ΔN_t is the total excess electron content of the transient material along the signal ray path,

$$\Delta N_t = \int_t \Delta n \,\mathrm{d}s \,, \tag{7}$$

and $\overline{\mathbf{B}}_L$ is the weighted mean longitudinal (line-of-sight) component of the magnetic field in the transient:

$$\overline{B}_L = \frac{1}{N_t} \int_t n_t \mathbf{B}_t \,\mathrm{ds}; \quad N_t = \int_t n_t \,\mathrm{d}s \,. \tag{8}$$

Values of ΔN_t at the Helios line-of-sight were determined from an interpolation procedure using all available 'Solwind' difference images. These columnar electron densities were then used in (6) to compute $\overline{B}_L$ at 30 min intervals. The results are presented in Table I.

TABLE I

Transient magnetic field estimates

1979 Date	UT	Solar offset ($R_\odot$)	ΔN_t (10^{16} cm^{-2})	ΔFR (degrees)	$\overline{B}_L$ (mG)
23 Oct.	12 : 00	7.5	0.2	± 5	± 10
	12 : 30	7.4	0.3	10	13
	13 : 00	7.4	0.4	± 5	± 5
	13 : 30	7.3	0.5	± 5	± 4
	14 : 00	7.3	0.6	− 10	− 7
	14 : 30	7.2	0.8	− 35	− 17
	15 : 00	7.1	1.0	− 60	− 23
24 Oct.	08 : 00	5.1	1.8	± 10	± 2
	08 : 30	5.1	1.8	20	4
	09 : 00	5.0	1.9	40	8
	09 : 30	5.0	1.9	55	11
	10 : 00	4.9	2.0	35	7
	10 : 30	4.9	2.0	± 5	± 1
	11 : 00	4.8	2.0	− 45	− 9

The maximum magnitudes for the mean longitudinal component of the transient magnetic field were found to lie in the range 10–25 mG. These values were compared with the total magnitude of the pre-transient magnetic field using the potential-field calculations based on Stanford mean solar field data (Hoeksema *et al.*, 1983). A contour map of the (assumed purely radial) field strengths on a source surface at 2.5 $R_\odot$ during the interval October/November 1979 was provided for this study by T. Hoeksema. These results indicate that the proximate point along the Helios ray path was located very close to a magnetic sector boundary on the solar west limb during both events. The ambient field strengths in the pre-transient corona were thus determined to be relatively low. Assuming an inverse-square decrease in B_{amb} from 2.5 $R_\odot$ out to the radial distance of the Helios ray path, values of $B_{\text{amb}} \simeq 1$ mG were inferred for both CMEs.

Evidence for magnetic field reversals within the CMEs are also apparent from Table I. The reversal in ΔFR from 1000 to 11 : 00 UT on 24 October, which occurred during an interval of minimal variation in ΔN_t, is the most convincing example of this effect.

For the two transient events investigated here, the derived values of $\overline{B}_L$ were found to be of the same order as, or perhaps marginally greater than, the total ambient field strength B_{amb} derived from independent potential field calculations. The transient fields were typically 10–100 mG when scaled with a radial dependence R^{-2} to a nominal solar

distance of 2.5 $R_\odot$. This can be compared with the 2–4 G at the same coronal heights derived from radio burst observations (Dulk *et al.*, 1976; Gergely *et al.*, 1979).

As shown by Bird *et al.* (1980), values of $\overline{B}_L$ of the order of 2–4 G would produce thousands of degrees of Faraday rotation at S-band. No such event has been seen in over 1200 hr of Helios FR data taken inside 15 $R_\odot$ since 1975. One example reported here (Helios 1: 16 November 1979) did display a FR profile similar to that expected from a helical magnetic flux loop moving through the Helios/Earth line-of-sight. However, the magnetic field values $\overline{B}_L$ associated with this disturbance are not expected to be significantly higher than for the events given in Table I, because the amplitude of the FR oscillations was only $\pm 40°$. One possible explanation for the small field magnitudes shown in Table I might be that the transient fields are incoherently ordered, or at least randomly oriented on scales smaller than the thickness of the CME. This would cause considerable cancellation along the integral in (3), thereby yielding a smaller value for ΔFR.

5. Summary

Simultaneous white-light and radio sounding observations of the solar corona were made during the solar occultations of the two Helios spacecraft in October/November 1979. Five coronal disturbances were recorded during these intervals by the radio sounding data and each could be associated either directly or indirectly with coronal mass ejection events seen in 'Solwind' coronagraph images. The Faraday rotation of the Helios signal was seen to exhibit abrupt discontinuities during each event. Some events were characterized by quasi-periodic oscillations that can be explained only by polarity reversals of the transient magnetic fields.

The magnitude of the transient Faraday rotation yields values for the longitudinal component of the transient magnetic field in the range 10–100 mG (scaled to 2.5 $R_\odot$). These fields were still somewhat greater than the estimated ambient field strength for the two events studied. The values of the transient magnetic fields from these measurements refer to only one component of the total field, and even this component may be moderated by cancellation effects along the line-of-sight through the coronal transient. This possible discrepancy with the much larger transient field magnitudes inferred from radio burst observations (2–4 G at 2.5 $R_\odot$) could probably only be resolved with comprehensive white-light and Faraday rotation observations of a more massive and internally structured (loop-like or otherwise) coronal mass ejection under more favorable geometrical conditions.

Appendix

The expression (5) for the transient Faraday rotation ΔFR is examined here in detail, in particular to determine under what circumstances the approximation (6) is justified. The quantity of interest to this investigation, the mean weighted magnetic field of the coronal transient, is defined by (8). Using this definition, (5) was seen to be a sum of

three terms:

$$\Delta FR = T_1 + T_2 + T_3 , \tag{A1}$$

where

$$T_1 = K\bar{B}_L \Delta N_t , \tag{A2}$$

$$T_2 = K\bar{B}_L \; N_0 , \tag{A3}$$

$$T_3 = -K \int_t n_0 \mathbf{B}_0 \, \mathbf{ds} . \tag{A4}$$

The excess columnar electron content ΔN_t and the ambient columnar electron content N_0 are defined by

$$\Delta N_t = \int_t \Delta n \, \mathrm{d}s, \tag{A5}$$

or

$$N_0 = \int_t n_0 \, \mathrm{d}s. \tag{A6}$$

The term T_2 arises because the coronagraph image differencing yields the *excess* electron content of the transient, not the *total* electron content. It is not possible to measure the ambient (or total) electron content along the integration path segment in the CME. Since the integrals (A5) and (A6) are taken over the same path length, neglect of (A3) with respect to (A2) is tantamount to the approximation $\Delta n \gg n_0$. The term T_3 is due to removal of the ambient contribution along the integration path occupied by the CME. Estimates of T_2 and T_3 can only be computed from models of the ambient electron density distribution. Both correction terms are also seen to be linearly proportional to the longitudinal extent L of the CME. The relative importance of T_2 and T_3 will thus be greatest when the transient occupies the largest possible segment of the signal ray path.

The generalized geometry of the occultation of a CME by the Helios radio signal is shown in an ecliptic plane view in Figure 14. The proximate point along the signal ray path (solar offset) is located a distance R from the Sun. The coronal transient has a total thickness L along the radio ray path and is centered at s_0 as measured from the limb plane of the Sun.

The pre-transient coronal electron density and magnetic field are given by

$$n_0 = n(R) \left(\frac{R^2}{r^2}\right) = n(R) \left(\frac{R^2}{R^2 + s^2}\right), \tag{A7}$$

$$\mathbf{B}_0 = B_r \mathbf{r}, \qquad B_r = B_0(R, s) \left(\frac{R^2}{R^2 + s^2}\right), \tag{A8}$$

where $n\,(R)$ determines the general level of the ambient electron density. The model of Beard (1979) for the solar equator at solar maximum was used in the following

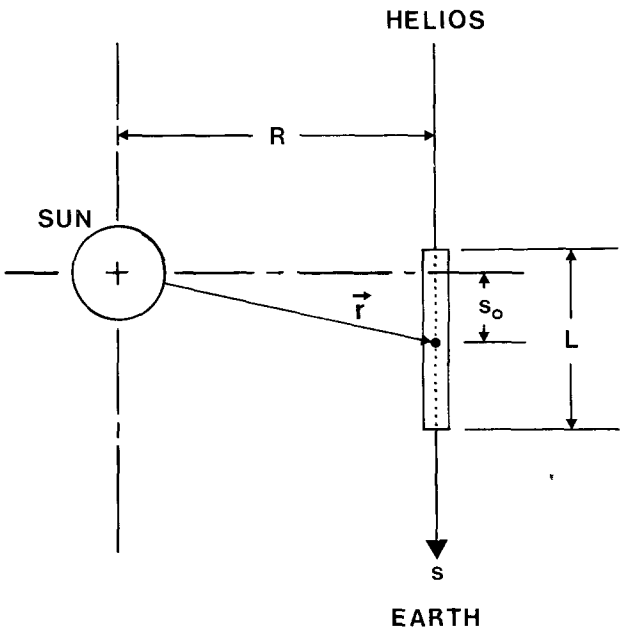

Fig. 14. Occultation geometry of a CME by the Helios/Earth line-of-sight (ecliptic plane view). Position along the Helios ray path, passing the Sun by a distance R, is denoted by s. The center of the CME is located at s_0; its longitudinal extent along the ray path is given by L.

calculations. The longitudinal dependence of $B_0(R, s)$ in (A8) was chosen such that the ambient field's polarity yielded the maximum contribution to ΔFR, i.e. no cancellation along the integration path:

$$B_0(R, s) = \begin{cases} B_0(R), & s > 0, \\ -B_0(R), & s < 0. \end{cases} \tag{A9}$$

The magnitude of $B_0(R)$ was inferred from the potential-field calculations (Hoeksema, priv. communication) described earlier. Both the electron density and the magnetic field of the pre-transient corona were assumed to have an inverse-square radial dependence at those solar offsets of interest to this analysis ($r > 4.5\ R_\odot$).

Substituting (A7) into (A6), one obtains:

$$N_0 = n(R)R\left\{\tan^{-1}\left(\frac{s_0 + L/2}{R}\right) - \tan^{-1}\left(\frac{s_0 - L/2}{R}\right)\right\}. \tag{A10}$$

If the transient is located close to the limb plane and is not greatly extended along the line-of-sight, then the approximation $|s_0 \pm L/2| \ll R$ can be applied to (A10) to yield:

$$N_0 \simeq n(R)L\{1 - (s_0/R)^2\}. \tag{A11}$$

Using (A7) and (A8) in the expression for T_3 (A4), one must distinguish between two possible cases:

Case 1: $s_0 \leq L/2$ (transient intersects limb plane); then

$$T_3 = \frac{Kn(R)RB_0(R)}{3}\left\{2 - \left[1 + \left(\frac{s_0 - L/2}{R}\right)^2\right]^{-3/2} - \left[1 + \left(\frac{s_0 + L/2}{R}\right)^2\right]^{-3/2}\right\}; \tag{A12}$$

Case 2: $s_0 \geq L/2$; then

$$T_3 = \frac{Kn(R)RB_0(R)}{3}\left\{\left[1 + \left(\frac{s_0 - L/2}{R}\right)^2\right]^{-3/2} - \left[1 + \left(\frac{s_0 + L/2}{R}\right)^2\right]^{-3/2}\right\}. \tag{A13}$$

In order to evaluate the importance of T_2 and T_3, values are needed for the parameters s_0 and L in addition to $n(R)$ and $B_0(R)$. The thickness of the transient along the line-of-sight was taken to be equal to its measured extent in *latitude* at the distance of the Helios ray path. This approach assumes the CME to be 'bubble-like' in shape. The values of L are thus expected to be close to the maximum expected, resulting in relatively larger correction terms T_2 and T_3. Both CMEs in this study were located close to the solar limb ($s_0 \simeq 0$). This location tends to maximize T_2 via (A10), but T_3 reaches its maximum for transients with $s_0 = L/2$ (Case 1), and $s_0 \simeq R/2$ (Case 2). Since the exact position cannot be determined from the 'Solwind' images, these three values for s_0 were used for the test calculations of T_2 and T_3.

The magnitude of the three terms of (A1) are compared for the two specific times during the CMEs of 23 and 24 October in Table II. The times were selected when ΔN_t

TABLE II

Relative magnitudes of correction terms to Equation (5)

	Event date: UT	
	23 Oct., 1979: 1500	24 Oct., 1979: 1100
$R, R_\odot$	7.1	4.8
$L, R_\odot$	3.5	2.0
$n(R)$, cm^{-3}	3.0×10^4	1.1×10^5
$B_0(R)$, mG	1	1
T_1, deg, S-band	−60	−45
$\lvert T_2/T_1 \rvert$		
$s_0 = 0$	0.73	0.76
$s_0 = L/2$	0.69	0.73
$s_0 = R/2$	0.55	0.57
$\lvert T_3/T_1 \rvert$		
$s_0 = 0$	0.004	0.009
$s_0 = L/2$	0.006	0.015
$s_0 = R/2$	0.008	0.024

was close to maximum, but the values of L at earlier times would be expected to be smaller as well, thus not significantly increasing the relative magnitudes of T_2 of T_3. Including the value of T_2 in the calculation of $\bar{B}_L$ is seen to result in a downward correction of about 40%. Since neglecting T_2 is equivalent to an underestimate of the transient electron content, this correction will always result in a decrease in the computed $\bar{B}_L$. The term T_3 is determined to be negligible for all possible values of s_0 and would still be of only minor importance even for ambient field strengths ten times larger than those assumed in Table II.

References

Anzer, U. and Pneuman, G. W., *Solar Phys.* **79**, 129.

Beard, D. B.: 1979, *Astrophys. J.* **234**, 696.

Bird, M. K., Volland, H. Stelzried, C. T., Levy, G. S., and Seidel, B. L.: 1977, in M. A. Shea *et al.* (eds.), *Contributed Papers to the Study of Travelling Interplanetary Phenomena/1977*, AFGL-TR-77-0309, p. 63.

Bird, M. K., Volland, H., Seidel, B. L., and Stelzried, C. T.: 1980, in M. Dryer and E. Tandberg-Hanssen (eds.), *Solar and Interplanetary Dynamics*, D. Reidel Publ. Co., Dordrecht, Holland, p. 475.

Bird, M. K., Volland, H., Howard, R. A., Koomen, M. J., Michels, D. J., Sheeley, Jr., N. R., Armstrong, J. W., Seidel, B. L., Stelzried, C. T., and Woo, R.: 1984, in M. A. Shea *et al.* (eds.), *STIP Symposium on Solar/Interplanetary Intervals*, Engineering International Inc., Huntsville, p. 101.

Burlaga, L. F., Klein, L., Sheeley, Jr., N. R., Michels, D. J., Howard, R. A., Koomen, M. J., Schwenn, R., and Rosenbauer, H.: 1982, *Geophys. Res. Letters* **12**, 1317.

Crifo, F., Picat, J. P., and Cailloux, M.: 1983, *Solar Phys.* **83**, 143.

Dryer, M.: 1982, *Space Sci. Rev.* **33**, 233.

Dulk, G. A., Smerd, S. F., MacQueen, R. M., Gosling, J. T., Magun, A., Stewart, R. T., Sheridan, K. V., Robinson, R. D., and Jacques, S.: 1976, *Solar Phys.* **49**, 369.

Gergely, T. E., Kundu, M. R., Munro, R. H., and Poland, A. I.: 1979, *Astrophys. J.* **230**, 575.

Hoeksema, J. T., Wilcox, J. M., and Scherrer, P. H.: 1983, *J. Geophys. Res.* **88**, 9910.

House, L. L., Wagner, W. J., Hildner, E., Sawyer, C. B., and Schmidt, H.: 1981, *Astrophys. J. Letters* **244**, L117.

Howard, R. A., Michels, D. J., Sheeley, Jr., N. R., and Koomen, M. J.: 1982, *Astrophys. J. Letters* **263**, L101.

Howard, R. A., Sheeley, Jr., N. R., Koomen, M. J., and Michels, D. J.: 1985, *J. Geophys. Res.* (in press).

Levy, G. S., Sato, T., Seidel, B. L., Stelzeried, C. T., Ohlson, J. E., and Rusch, W. V. T.: 1969, *Science* **166**, 596.

Low, B. C.: 1981, *Astrophys. J.* **251**, 352.

MacQueen, R. M.: 1980, *Phil. Trans. Roy. Soc. London* **A297**, 605.

Mouschovias, T. C. and Poland, A. I.: 1978, *Astrophys. J.* **220**, 675.

Pneuman, G. W.: 1980, *Solar Phys.* **65**, 369.

Pneuman, G. W.: 1983, *Astrophys. J.* **265**, 468.

Schwenn, R.: 1983, *Space Sci. Rev.* **34**, 85.

Sheeley, Jr., N. R., Michels, D. J., Howard, R. A., and Koomen, M. J.: 1980a, *Astrophys. J.* **237**, L99.

Sheeley. Jr., N. R., Howard, R. A., Koomen, M. J., Michels, D. J. and Poland, A. I.: 1980b, *Astrophys. J.* **238**, L161.

Sheeley, Jr., N. R., Howard, R. A., Koomen, M. J., Michels, D. J., Schwenn, R., Muhlhauser, K. H., and Rosenbauer, H.: 1983, in M. Neugebauer (ed.), *Solar Wind Five*, NASA-CP 2280, p. 693.

Sheeley, Jr., N. R., Stewart, R. T., Robinson, R. D., Howard, R. A., Koomen, M. J., and Michels, D. J.: 1984, *Astrophys. J.* **279**, 839.

Steinolfson, R. S., Wu. S. T., Dryer, M., and Tandberg-Hanssen, E. : 1978, *Astrophys. J.* **225**, 259.

Stewart, R. T., Dulk, G. A., Sheridan, K. V., House, L. L., Wagner, W. J., Sawyer, C., and Illing, R.: 1982, *Astron, Astrophys.* **116**, 217.

Wagner, W. J.: 1984, *Ann. Rev. Astron. Astrophys.* **22**, 267.

Wagner, W. J., Hildner, E., House, L. L., Sawyer, C., Sheridan, K. V., and Dulk, G. A.: 1981, *Astrophys. J. Letters* **244**, L123.

Woo, R.: 1977, in M. A. Shea *et al.* (eds.), *Study of Travelling Interplanetary Phenomena/1977*, D. Reidel Publ. Co., Dordrecht, Holland, p. 81.
Woo, R. and Armstrong, J. W.: 1981, *Nature* **292**, 608.
Woo, R., Armstrong, J. W., Sheeley, Jr., N. R., Howard, R. A., Michels, D. J., and Koomen, M. J.: 1982, *Nature* **300**, 157.
Wu, S. T., Steinolfson, R. S., Dryer, M., and Tandberg-Hanssen, E.: 1981, *Astrophys. J.* **243**, 641.
Yeh, T.: 1982, *Solar Phys.* **78**, 287.